Pergamon

PII: S0301-9322(96)00052-3

Int. J. Multiphase Flow Vol. 23, No. 1, pp. 37–54, 1997

0301-9322/97 $17.00 + 0.00

LOCAL AND MEAN HEAT TRANSFER COEFFICIENTS IN BUBBLY AND SLUG FLOWS UNDER MICROGRAVITY CONDITIONS

R. W. RITE and K. S. REZKALLAH

Department of Mechanical Engineering, University of Saskatchewan, Saskatoon, SK S7N 5A9, Canada

(Received 12 January 1996; in revised form 21 July 1996)

Abstract—Experimental local heat transfer data were collected on-board NASA's KC-135 reduced gravity aircraft for two-phase, air–water flow in vertical, upward, co-current flow through a 9.53 mm circular tube. It was found that in the bubbly and slug flow regimes (surface tension dominated regimes) reduced gravity has a tendency to lower the heat transfer coefficient by as much as 50% at the lowest gas qualities. As the gas-quality increases (transition to annular flow), the difference between the $1-G$ and $\mu-G$ heat transfer coefficients is much less significant. Due to minimal slip between the two-phases at $\mu-G$ conditions and a thermal entry length heat transfer coefficient profile similar to that for single-phase flows, it is proposed to predict the two-phase heat transfer coefficients with analytical single-phase thermal entry length solutions. This method was found to predict coefficients within $\pm 26\%$ for bubbly and slug flow regimes for $3000 < Re_{TP} < 10{,}000$ using superficial liquid Reynolds numbers. For $Re_{TP} > 10{,}000$, empirical single-phase turbulent correlations provide a reasonable match to the experimental data. Copyright © 1996 Elsevier Science Ltd.

Key Words: two-phase flow, microgravity, heat transfer, thermal entry length

1. INTRODUCTION

Over the remaining years in this decade and into the next century, the need for space-based systems such as satellites for communications and research purposes as well as manned space-platforms is expected to grow exponentially. The capabilities of these systems and, hence, their power requirements will also increase due to the forecasted escalating power demands. This means more sophisticated thermal management systems with greater heat capacities must be designed. One way in which such high thermal transport demands may be met is through the use of two-phase systems.

Two-phase systems have been utilized and researched in the petrochemical and nuclear industries for many decades. However, the knowledge-base for their use in space hardware has only recently been accumulating. Some experimental studies of two-phase convective heat transfer were performed under microgravity conditions, mostly for single-component flows (i.e. boiling and condensation). Among these are the studies by Papell (1962) and Feldmanis (1966). In his study, Papell reported a 15% increase in the heat transfer rate for a subcooled water system during reduced gravity duration on-board NASA's KC-135 aircraft. Feldmanis (1966) did not explicitly determine heat transfer coefficients, but based on temperature measurements that were made during his experiment, he predicted that for forced convective condensation gravity would have little influence on the heat transfer rate and that boiling heat transfer coefficients would be higher at $\mu-G$.

More recently, Reinharts *et al.* (1992) worked with a boiling and condensing Refrigerant-12 test loop on-board NASA's KC-135. They reported that the condensation heat transfer coefficients were 26% lower for $\mu-G$ conditions as opposed to $1-G$ conditions. Boiler temperatures remained constant throughout the KC-135 flights. Thus, no conclusions were drawn on the effect of gravitational acceleration on the boiling heat transfer coefficients. Ohta *et al.* (1994) completed a study of Refrigerant-113 in a convective boiling system with vertical, upward flow through a 8 mm i.d. circular tube. The mass velocity ranged from 150 to 600 kg/m^2 s, and the gas quality was changed from 0.0 to 0.5. Parabolic flight aboard the NASDA MU-300 were used to generate the microgravity conditions. They reported that while boiling was occurring (vigorous bubble

nucleation at the heated wall) in the bubbly and annular flow regimes there was no difference in the heat transfer coefficients between $1 - G$ and $\mu - G$ conditions. However, when boiling was minimized by high flow rates and low heat flux, the heat transfer coefficients were lower at $\mu - G$ as compared with $1 - G$. They attributed this decrease to a reduction in the turbulence intensity at the liquid–vapor interface and an increase in the film thickness. The authors reported that, based on video images that were recorded, those changes were precipitated by an absence of disturbance waves at the surface.

From the studies cited above with their conflicting results, it is clear that further experimental investigation into the heat transfer behavior of two-phase flows under $\mu - G$ is warranted.

2. EXPERIMENTAL METHODS

2.1. Experimental apparatus

A two-phase, two-component test apparatus was designed and built for the performance of microgravity experiments on NASA's KC-135 Zero-g aircraft. The apparatus is instrumented such that simultaneous measurements of pressure drop and heat transfer data can be made, as well as continuous observation and recording of the two-phase flow patterns. In order to cover a wide range of test conditions, the facility allows for the independent control of three separate parameters during testing: air flow rate, water flow rate, and the temperature of the two-phase mixture at different locations in the flow loop.

A schematic of the test apparatus is shown in figure 1. The apparatus was situated such that the heated test section was oriented vertically with respect to the floor of the aircraft. A complete discussion of the flow loop may be found in Rite and Rezkallah (1993). In addition, more details concerning the heated test section (which is of primary importance in this work) will be provided here.

In the mixer shown at the lower left-hand side of the schematic, air is injected radially while water flows axially. The two-phase mixture then proceeds through a 74 cm long flow developing section with an inside diameter of 9.53 mm ($L/D \approx 77$). A 16.2 cm long ($L/D \approx 17$) observation section follows as shown in the figure. The observation section is constructed of a 9.53 mm i.d. acrylic tube. Thus, from the exit of the mixer to the heated test section, the total calming length is 110 D. This provides for a fully developed velocity profile before heat transfer measurements are taken along the heated test section.

Following the observation section, the temperature of the mixture is measured with a 3.18 mm diameter, 10 cm long platinum, Resistance Temperature Device (RTD) which is inserted transversely into the flow. In order to minimize any interference with the flow, which could cause a distortion of the flow pattern, a special fixture was designed for the RTD. The fixture consists of an acrylic Tee section with a 9.53 mm i.d. for the straight through section and a 6.35 mm i.d. branch. In the branch, an RTD is inserted such that its tip is flush with the inner wall of the straight through section. This allows the entire length of the probe to be immersed in the two-phase mixture, but at the same time minimizes the disturbance to the flow.

The inlet temperature RTD fixture is followed by the heated test section. It consists of a 9.53 mm i.d. copper tube having a wall thickness of 1.59 mm. The copper tube has a total length of 39.4 cm of which 35.6 cm are heated. Twelve copper-constantan thermocouples were soldered to the copper tube and used for the surface temperature measurement. The heater wire is a 28 gauge varnished copper wire. The wrapping was done in two separate sections wired in parallel in order to allow for the necessary power requirements without exceeding the amount of available amperage on-board the aircraft. This permits up to 1000 W of total heat addition to the two-phase mixture for a maximum power flux of 94 kW/m^2. In order to minimize heat losses to the ambient from the heater during operation, 50 mm of a high temperature, ceramic fiber insulation was packed around the heater. In addition, a 20 mm thick blanket of fiberglass insulation was wrapped around the entire structure. The latter was covered with an aluminum sheet metal casing. At the outlet of the heated test section, another 3.18 mm RTD is used to measure outlet temperature. This temperature probe is inserted axially into the outlet flow, allowing for complete immersion in the gas–liquid mixture. Interference with the flow pattern was not a consideration here.

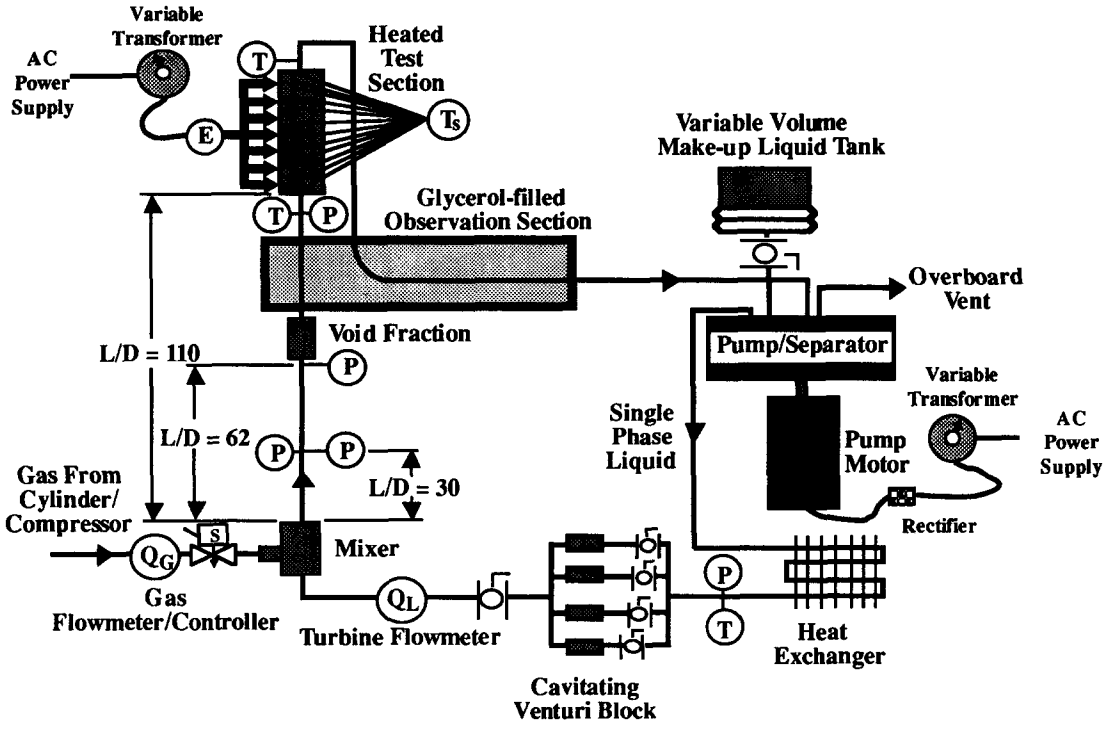

Figure 1. Schematic of two-phase flow flight test facility.

All data acquisition functions were handled by a 80486-based PC equipped with 12-bit analog-to-digital conversion using a successive approximation algorithm. A C++ computer program was used to acquire the heat transfer data once every 0.03 s and to control the air flow rate.

2.2. *Experimental procedure*

NASA's KC-135 aircraft was utilized in order to obtain the reduced gravity conditions required. The KC-135 provides approximately 23 s of low-gravity per each parabola in the Keplerian flight trajectory. A typical flight consists of four sets of ten parabolas each. Four flight campaigns aboard the aircraft were conducted for a total of 16 flights during which useful heat transfer information was collected. A summary of the range of flow velocities and Reynolds numbers gathered during flights is shown in table 1. In the table, V_{SL} and V_{SG} are the superficial liquid and gas velocities, respectively. Superficial velocity being the volumetric flow rate of the liquid or the gas divided by total flow area. The superficial liquid and gas Reynolds numbers are defined as:

$$\mathrm{Re}_{SL} = \frac{\rho_L V_{SL} D}{\eta_L} \quad [1]$$

$$\mathrm{Re}_{SG} = \frac{\rho_G V_{SG} D}{\eta_G} \quad [2]$$

where ρ_L and ρ_G are the liquid and gas densities (kg/m^3), respectively; D is the inner tube diameter (m); η_L is the liquid dynamic viscosity (N s/m^2); and η_G is the viscosity of the gas phase (N s/m^2).

At microgravity, on average, the pressure at the inlet to the test section was 84.4 kPa over the range of liquid and gas flow rates shown in table 1. The change of the pressure inside the aircraft

Table 1.

V_{SL} (m/s)	V_{SG} (m/s)	Re_{SL}	Re_{SG}
0.04–3.70	0.09–26.00	466–61,333	43–12,932

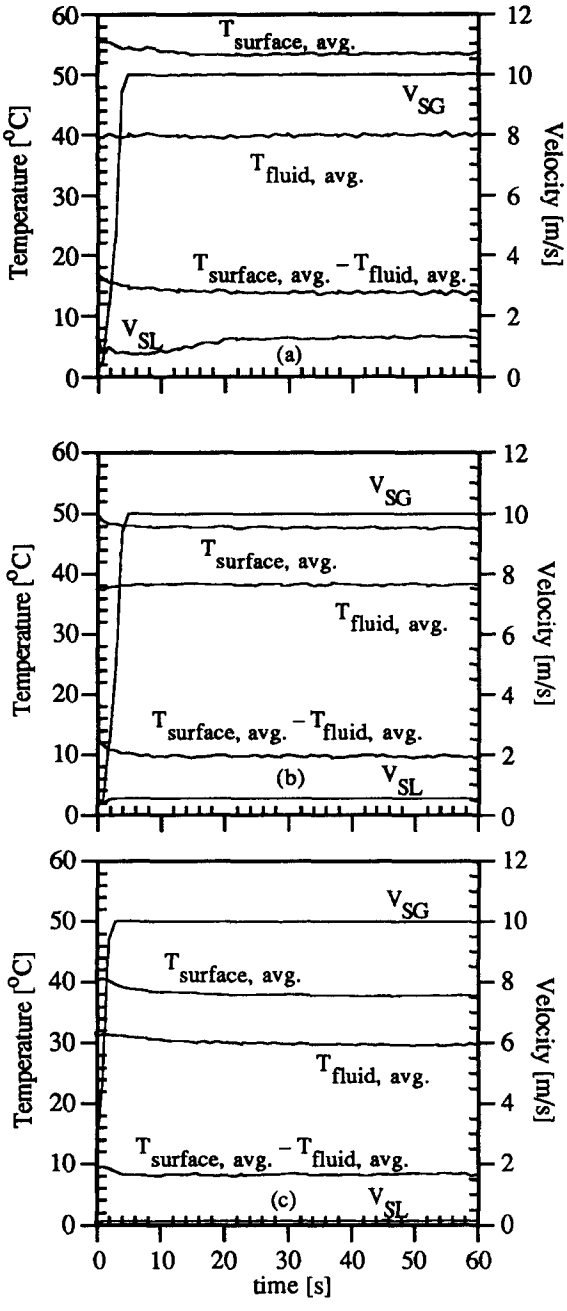

Figure 2. Thermal response of heated test section with flow regime transition.

was less than 15% during the climb-up and descending periods of the parabolic flights. Thus, the influence of such small changes on the measurements can be neglected.

In total, 433 flight data points were recorded over the 16 flights with approximately an equal number of points recorded on-ground in the laboratory. These data points were mostly for air–water mixtures. However, data were also collected with three air–glycerol/water mixtures of 50% glycerol, 59% glycerol, and 65% glycerol by weight, respectively. The results for these high viscosity mixtures can be found in Rite and Rezkallah (1994b).

2.3. Data reduction

The independent measurements in this study were the flow rates of the liquid and gas phases and the heat flux at the surface of the heated test section, while the dependent measurements were

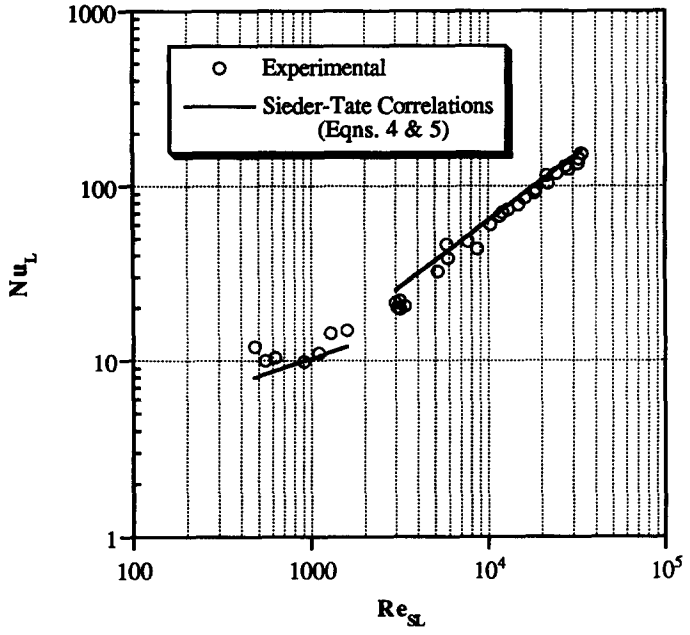

Figure 3. Comparison of single-phase experimental data with Sieder–Tate correlations: laminar and turbulent flows.

the temperatures along the heated surface and the bulk fluid temperature. During the flights, measurements were collected continuously during the low-gravity portions of each parabola. The collected data then averaged over time for each parabola. Before the averaging process was performed, three conditions were imposed on the independent variables collected for each data point. These conditions were: (1) the liquid and gas flow rates (or velocities) and heater power had minimum fluctuation for the duration of data collection (less than 7%); (2) the gravity-level was between ± 0.04 of standard earth gravity (g_0); and (3) quasi-steady-state conditions for heat transfer measurements existed.

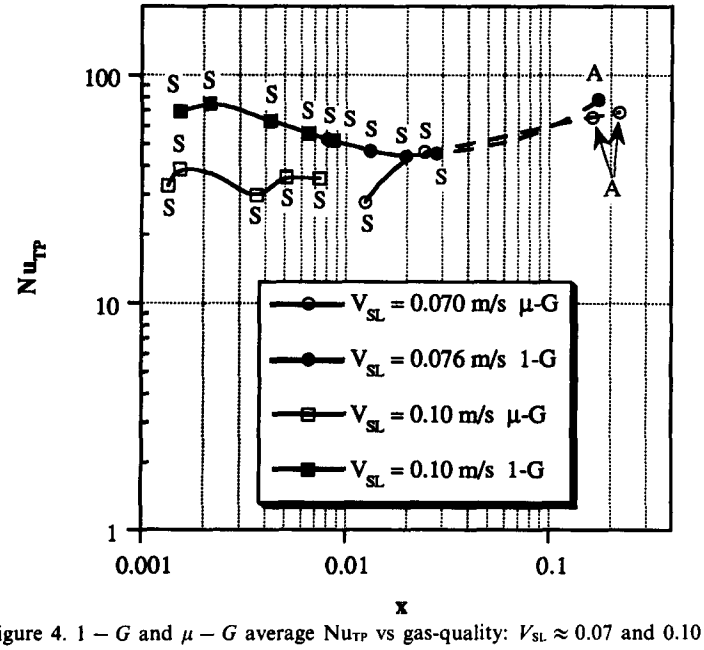

Figure 4. $1-G$ and $\mu-G$ average Nu_{TP} vs gas-quality: $V_{SL} \approx 0.07$ and 0.10 m/s.

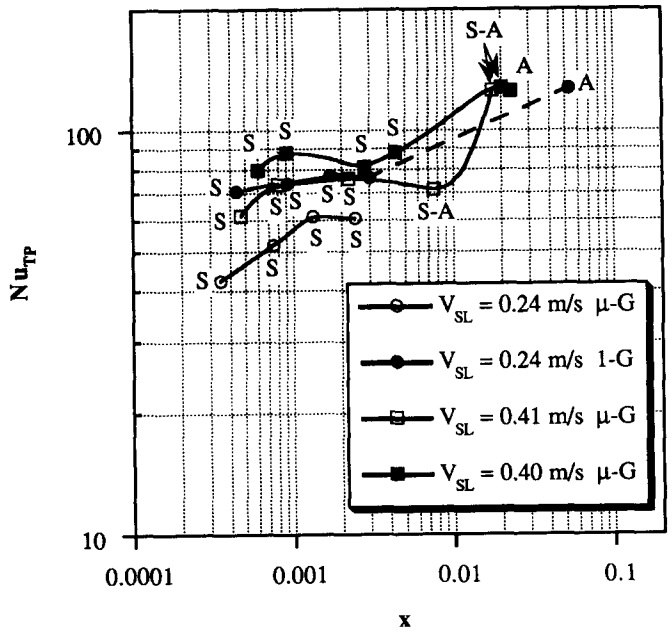

Figure 5. $1-G$ and $\mu-G$ average Nu_{TP} vs gas-quality: $V_{SL} \approx 0.24$ and 0.41 m/s.

The quasi-steady-state condition addresses the question of whether the time response of the heated test section and the flow is such that steady-state thermal conditions could be achieved given the short duration of reduced gravity on-board the flight aircraft. This was investigated experimentally, first on-ground and later during the course of the first flight campaign. The results from ground tests are presented in figure 2. In that experiment, the gas flow was increased instantaneously in order to precipitate a flow regime transition. The results at $V_{SL} = 1.2$, 0.5, and 0.1 m/s are shown in figure 2 (a)–(c). In the figure, the average surface temperature of the heated test section, the average bulk fluid temperature of the mixture in the test section and the difference between them, as well as the superficial gas and liquid velocities are plotted for 60 s after an increase in the gas velocity at time = 0 from 0.2 to 10 m/s. In each of these cases, a gas velocity change

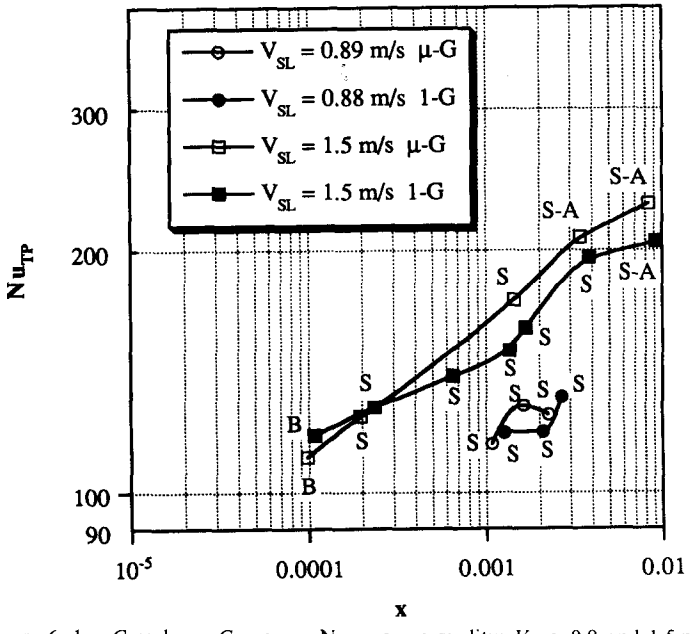

Figure 6. $1-G$ and $\mu-G$ average Nu_{TP} vs gas-quality: $V_{SL} \approx 0.9$ and 1.5 m/s.

Table 2.

Data point	Flow regime	g/g_0	V_{SL} (m/s)	V_{SG} (m/s)	Re_{SL}	Re_{SG}	x	ϵ	Nu_{TP}	ψ^2	q'' (W/m²)	
F3P3	S	9.99E-04	0.05	0.19	538.0	88.2	3.82E-03	—	17.6	2.18	14838.2	
F3P4	S	9.29E-04	0.04	0.39	466.3	179.3	9.17E-03	—	17.9	2.35	14683.3	
F3P6	S	5.18E-03	0.10	0.14	1179.3	66.7	1.34E-03	0.56	32.9	3.19	17839.8	
F3P7	S	− 4.08E-03	0.11	0.19	1361.9	89.9	1.53E-03	0.56	38.8	3.57	17880.2	
F3P8	S	1.13E-03	0.10	0.39	1173.8	182.4	3.65E-03	0.73	29.8	2.88	17882.4	
F3P9	S	4.47E-03	0.11	0.59	1282.3	275.6	5.08E-03	0.77	35.8	3.38	1.7861.3	
F3P10	S	1.14E-03	0.10	0.79	1179.8	367.4	7.40E-03	0.71	35.4	3.45	17799.6	
F3P12	S	− 2.62E-02	0.24	0.09	2863.0	43.2	3.47E-04	0.39	42.4	1.77	19587.6	
F3P13	S	− 9.63E-03	0.24	0.19	2850.3	91.4	7.44E-04	0.44	51.9	2.18	22934.9	
F3P14	S	− 3.71E-03	0.24	0.34	2871.1	160.5	1.33E-03	0.62	61.2	2.58	27964.9	
F3P15	S	3.16E-03	0.24	0.64	2971.7	301.6	2.42E-03	0.69	60.6	2.49	27887.4	
F3P16	S	− 2.17E-03	0.13	0.09	1594.3	42.9	6.68E-04	—	40.2	3.56	27563.2	
F3P17	S	− 8.22E-03	0.38	0.19	4543.2	91.1	4.70E-04	0.39	61.4	1.78	31919.4	
F3P18	S	− 4.31E-03	0.40	0.34	4762.1	162.4	8.04E-04	0.42	73.4	2.05	36756.9	
F3P19	S	− 101E-02	0.29	0.49	3540.0	231.5	1.59E-03	0.66	65.2	2.33	36657.9	
F3P22	B	4.58E-03	0.85	0.09	10681.6	43.1	1.00E-04	0.14	74.2	1.11	25335.5	
F3P24	B	1.16E-02	0.71	0.19	8941.2	91.2	2.53E-04	0.17	76.5	1.32	27735.5	
F3P25	B	− 4.89E-03	0.80	0.39	10192.7	189.7	4.66E-04	0.22	90.1	1.41	30732.6	
F3P26	B	8.61E-03	0.97	0.09	12474.9	43.7	8.92E-05	0.17	81.1	1.08	30511.9	
F3P27	B	− 2.68E-03	1.45	0.14	18522.0	72.1	9.79E-05	0.12	110.6	1.08	30477.0	
F3P28	B	8.97E-03	1.17	0.19	15191.8	94.1	1.59E-04	0.13	104.1	1.19	36272.8	
F3P29	B	− 6.23E-03	1.50	0.29	19334.5	148.7	1.96E-04	0.14	124.6	1.18	36364.0	
F3P30	B	− 1.19E-02	1.17	0.39	15392.0	193.8	3.29E-04	0.18	111.5	1.27	37485.5	
F3P32	B	− 1.12E-03	2.47	0.09	32378.3	51.9	4.16E-05	0.12	154.6	0.97	47799.9	
F3P33	B	− 2.08E-03	2.52	0.15	33796.9	81.4	6.42E-05	0.11	162.3	0.99	47689.7	
F3P34	B	7.03E-03	2.50	0.19	34238.0	107.8	8.62E-05	0.11	166.7	1.02	59231.1	
F3P35	B	2.25E-03	2.49	0.24	34005.2	137.1	1.10E-04	0.12	168.6	1.03	59273.2	
F3P36	B	− 1.69E-02	2.52	0.29	35512.1	165.4	132E-04	0.13	182.6	1.09	70843.9	
F3P37	B	− 1.09E-02	2.46	0.39	35548.0	220.6	1.81E-04	0.13	183.2	1.11	704.57.1	
F4P12	S	1.05E-02	0.13	0.96	1436.9	469.0	7.23E-03	0.66	66.5	6.04	12782.9	
F4P13	S	− 2.85E-04	0.11	1.95	1457.3	937.1	1.60E-02	0.57	78.6	7.34	45066.0	
F4P15	A	5.28E-03	0.04	6.95	567.5	3027.7	1.48E-01	—	35.7	4.91	43578.6	
F4P16	A	4.26E-03	0.12	9.95	1660.5	4992.6	7.63E-02	—	78.1	7.20	43620.5	
F4P18	A	− 5.63E-04	0.10	13.95	1379.2	6931.4	1.18E-01	0.87	82.0	7.94	48493.9	
F4P22	S	− 1.44E-03	0.19	0.96	2577.2	445.8	4.65E-03	0.72	57.8	2.77	51722.3	
F4P23	S	− 1.60E-02	0.20	1.47	2738.4	672.3	6.77E-03	0.60	56.9	2.63	51579.4	
F4P24	S–A	5.69E-03	0.18	2.46	2430.2	1141.2	1.28E-02	0.63	66.8	3.39	51360.4	
F5P2	S	1.30E-02	0.10	0.55	1166.0	257.7	4.97E-03	0.74	32.5	3.07	27162.6	
F5P3	S	1.13E-03	0.07	0.96	839.1	449.7	1.24E-02	0.61	27.8	2.96	26135.3	
F5P5	S	2.02E-02	0.07	1.96	871.6	918.2	2.44E-02	0.64	46.2	4.93	28010.5	
F5P9	A	− 3.76E-03	0.07	13.92	852.5	7149.7	1.62E-01	0.88	65.8	7.03	33733.5	
F5P10	A	1.53E-02	0.07	17.86	795.4	10024.9	2.19E-01	—	69.1	7.47	36251.7	
F5P12	S	8.25E-03	0.41	0.97	4912.4	469.1	2.22E-03	0.67	75.9	2.07	27430.2	
F5P13	S	7.95E-03	0.32	1.47	3932.2	710.4	4.33E-03	—	73.9	2.41	46707.8	
F5P15	S–A	− 1.31E-02	0.46	3.48	5313.4	1809.4	7.60E-03	0.56	71.3	1.83	5788.9	
F5P16	S–A	4.29E-03	0.41	6.99	4816.5	3750.7	1.77E-02	0.68	125.4	3.48	42374.2	
F5P22	S	6.97E-03	0.88	0.96	10559.7	485.4	1.08E-03	0.50	115.0	1.70	49089.2	
F5P23	S	1.31E-02	0.91	1.46	11192.8	755.7	1.64E-03	0.58	128.5	1.84	49053.3	
F5P24	S	5.25E-03	0.88	1.96	11140.2	1003.1	2.26E-03	0.59	125.1	1.81	59347.4	
F5P34	S	− 2.95E-03	1.56	1.97	19823.6	1147.9	1.45E-03	0.52	173.8	1.61	34441.8	
F5P35	S–A	7.64E-03	1.47	3.96	19188.4	2568.0	3.45E-03	0.64	207.6	1.98	53714.3	
F5P40	S–A	3.04E-02	1.53	8.13	18399.6	6637.1	8.40E-03	0.73	227.9	2.19	32181.0	

induces a change in the flow pattern as follows: slug to annular for $V_{SL} = 1.2$ m/s, bubbly–slug transition to churn–annular transition for $V_{SL} = 0.5$ m/s, and slug–churn to annular for $V_{SL} = 0.1$ m/s.

It can be seen that as the liquid velocity increases the time required for steady-state temperatures to be achieved increases just as was found in Rite and Rezkallah (1993). This is expected since the thermal capacity of the two-phase mixture increases as the liquid flow rate increases. Thus, the thermal response of the heated test section will be slower as the heat capacity of the two-phase mixture is increased. However, it can also be seen that even in the worst case ($V_{SL} = 1.2$ m/s), the temperature difference between the surface and the bulk fluid essentially reaches its steady-state value after the first 10 s. Based on these findings, it was decided to use only the data collected during

the last 8–10 s of the microgravity portions of each parabola in order to minimize the impact of the thermal transient on the reported heat transfer measurements.

It was also shown (Rite and Rezkallah 1993) that in annular, slug–annular transition and slug flow regimes, the change of gravity had an effect on the heat transfer coefficients. However, in bubbly and bubbly–slug transition flows no change in the heat transfer coefficients was evident as the gravity level varied. More complete details on the above mentioned tests are presented in Rite and Rezkallah (1993) and Rite (1995).

Once the averaged data were obtained, the 12 measured surface temperatures $T_{s,i}$ were used to calculate the local convective heat transfer coefficients (h_i) from the equation:

$$h_i = \frac{E}{\pi LD(T_{s,i} - T_{b,i})} \quad [3]$$

where E is the total heat input into the test section (W), L is the length of the heated test section (m), and $T_{b,i}$ is the average bulk fluid temperature at the ith section of the heated tube (°C). Integration with respect to length then provided an average heat transfer coefficient (h_{TP}).

The Sieder–Tate correlations for single-phase laminar and turbulent flows were used to normalize the two-phase heat transfer coefficients, Kays and Perkins (1985) and Kakaç (1987). These

Table 3.

Data point	Flow regime	V_{SL} (m/s)	V_{SG} (m/s)	Re_{SL}	Re_{SG}	x	ϵ	Nu_{TP}	ψ^2	q'' (W/m²)
G3P2	S	0.05	0.09	499.0	55.6	2.37E-03	—	63.5	8.02	9997.0
G3P3	S	0.04	0.19	471.0	111.7	5.25E-03	—	50.9	6.61	13730.5
G3P4	S	0.03	0.39	320.8	223.3	1.53E-02	—	35.8	5.26	13573.3
G3P6	S	0.10	0.14	1124.9	79.9	1.53E-03	0.41	69.2	6.70	15421.9
G3P7	S	0.10	0.19	1149.6	112.4	2.16E-03	0.48	75.0	7.25	18967.0
G3P8	S	0.10	0.39	1169.3	224.9	4.26E-03	0.63	63.3	6.08	18928.7
G3P9	S	0.10	0.59	1146.5	334.9	6.55E-03	0.68	55.7	5.41	18857.7
G3P10	S	0.10	0.79	1163.3	445.3	8.63E-03	0.71	52.0	5.03	18737.9
G3P12	S	0.25	0.09	2886.9	55.7	4.40E-04	0.21	70.8	2.95	22862.5
G3P13	S	0.24	0.19	2865.0	113.6	9.13E-04	0.36	73.9	3.11	22826.4
G3P14	S	0.23	0.34	2758.2	197.9	1.69E-03	0.51	77.3	3.37	28127.4
G3P15	S	0.24	0.64	2894.0	364.2	3.00E-03	0.64	76.4	3.21	28098.3
G3P16	S	0.12	0.09	1478.1	54.7	9.17E-04	—	69.9	6.42	27842.2
G3P17	S	0.37	0.19	4734.5	113.7	5.99E-04	0.29	79.9	2.30	32213.8
G3P18	S	0.43	0.34	5514.4	198.5	9.11E-04	0.39	87.9	2.24	37934.9
G3P19	S	0.29	0.49	3752.6	278.0	1.90E-03	0.57	85.3	2.98	37797.4
G3P20	S	0.27	0.69	3584.0	387.0	2.79E-03	0.65	81.4	2.95	37713.7
G3P22	B	0.84	0.09	10657.9	55.2	1.29E-04	0.14	81.9	1.23	29736.1
G3P23	B	0.67	0.13	8482.5	77.6	2.29E-04	0.18	79.9	1.44	29629.5
G3P24	B	0.75	0.19	9578.1	113.4	2.97E-04	0.19	87.0	1.43	29604.5
G3P25	S	0.89	0.39	11370.7	233.8	5.20E-04	0.28	102.6	1.48	32780.4
G3P26	B	1.11	0.10	14293.2	58.0	1.04E-04	0.14	93.5	1.12	32763.6
G3P27	B	1.51	0.14	19706.4	82.1	1.08E-04	0.13	117.9	1.10	37715.6
G3P28	B	1.36	0.19	17793.7	116.8	1.71E-04	0.14	115.6	1.17	37659.7
G3P29	B	1.50	0.29	19821.4	178.7	2.36E-04	0.16	128.0	1.19	37716.2
G3P30	S	1.25	0.39	16529.8	236.6	3.75E-04	0.19	121.4	1.31	37846.8
G3P32	B	2.49	0.10	31594.9	62.2	4.95E-05	0.10	175.8	1.11	66023.0
G3P33	B	2.49	0.13	32777.4	87.9	7.02E-05	0.10	178.1	1.11	65727.2
G3P34	B	2.48	0.19	33635.8	126.1	1.01E-04	0.10	179.8	1.11	65223.6
G3P35	B	2.50	0.23	34780.2	152.6	1.22E-04	0.10	181.6	1.10	65354.0
G3P36	B	2.49	0.29	35817.6	191.3	1.55E-04	0.11	186.7	1.12	71536.4
G3P37	S	2.50	0.39	36655.3	257.6	2.08E-04	0.14	189.3	1.12	71279.0
G4P12	S	0.10	0.96	1178.7	548.4	1.03E-02	0.71	53.4	5.13	13727.3
G4P13	S	0.10	1.96	1282.0	1083.5	2.13E-02	0.69	59.4	5.71	47053.6
G4P14	C	0.13	3.96	1622.2	2241.6	3.28E-02	0.67	88.1	7.78	46366.0
G4P15	A	0.06	6.94	811.3	3794.6	1.12E-01	—	77.3	8.85	44693.9
G4P16	A	0.10	9.92	1244.3	5590.3	1.01E-01	—	90.5	8.79	45153.6
G4P17	A	0.09	11.92	1191.9	6718.7	1.25E-01	—	88.1	8.71	49058.7

Table 3—continued opposite

Table 3—*continued*

Data point	Flow regime	V_{SL} (m/s)	V_{SG} (m/s)	Re_{SL}	Re_{SG}	x	ϵ	Nu_{TP}	ψ^2	q'' (W/m²)
G4P18	A	0.10	13.93	1221.4	7943.1	1.41E-01	0.88	90.4	8.86	49172.0
G4P19	A	0.06	15.92	781.3	8999.9	2.26E-01	—	71.6	8.12	44931.5
G4P22	S	0.20	0.96	2558.8	536.4	5.35E-03	0.70	72.7	3.41	51638.4
G4P23	S	0.20	1.47	2608.8	813.2	8.17E-03	0.74	71.6	3.34	51710.1
G4P24	S	0.22	2.47	2913.2	1376.8	1.25E-02	0.68	78.5	3.37	52792.8
G4P26	A	0.13	6.94	1850.7	3800.5	5.48E-02	—	96.6	8.54	59535.5
G4P28	A	0.07	11.92	1060.0	6491.3	1.49E-01	—	78.8	8.39	56385.9
G5P2	S	0.08	0.56	947.9	313.8	8.08E-03	0.69	52.7	5.55	28072.9
G5P3	S	0.08	0.96	993.7	536.8	1.32E-02	0.74	46.8	4.85	27956.8
G5P4	S	0.08	1.41	971.7	786.5	1.98E-02	—	44.3	4.63	27786.9
G5P5	S	0.07	1.96	955.4	1088.0	2.80E-02	0.67	45.5	4.81	27836.4
G5P6	C	0.07	4.96	929.9	2745.8	7.09E-02	—	72.5	7.83	37280.8
G5P7	A	0.05	9.93	629.3	5523.2	1.83E-01	—	65.7	8.02	37388.2
G5P9	A	0.07	13.92	918.5	7975.0	1.74E-01	0.89	78.8	8.39	35288.9
G5P10	A	0.06	17.95	777.3	10707.5	2.48E-01	—	71.2	7.93	37740.6
G5P12	S	0.40	0.97	4836.6	568.1	2.78E-03	0.63	80.9	2.26	26815.9
G5P13	S	0.37	1.43	4643.1	829.1	4.38E-03	—	87.8	2.54	46593.3
G5P14	S	0.29	2.41	3718.1	1394.8	9.40E-03	0.67	86.9	3.03	46457.3
G5P15	S–A	0.53	3.40	6870.1	2036.9	7.60E-03	0.69	117.2	2.53	43199.4
G5P16	S–A	0.40	6.92	5187.0	4134.2	2.02E-02	0.72	127.6	3.46	43035.4
G5P17	S–A	0.28	9.92	3727.6	5837.3	3.96E-02	—	126.0	4.47	52104.3
G5P18	A	0.25	11.93	3327.5	7032.3	5.31E-02	—	126.9	4.94	51844.8
G5P19	A	0.27	13.88	3601.9	8352.6	5.80E-02	0.89	135.7	4.96	52034.5
G5P20	A	0.07	15.91	918.7	9027.6	2.03E-01	—	72.2	7.86	30593.3
G5P22	S	0.92	0.97	11658.9	593.2	1.27E-03	0.45	118.8	1.66	49579.1
G5P23	S	0.82	1.43	10600.9	867.4	2.09E-03	0.58	119.1	1.81	49261.2
G5P24	S	0.90	1.97	11956.2	1211.9	2.68E-03	0.62	131.7	1.84	59619.8
G5P25	S–A	0.70	3.97	9325.1	2459.3	7.00E-03	0.67	143.6	2.45	59912.0
G5P26	S–A	0.51	5.93	6902.9	3605.1	1.40E-02	—	140.8	3.08	59970.0
G5P27	A	0.40	7.93	5403.4	4719.6	2.31E-02	—	124.5	3.32	37705.0
G5P28	A	0.13	9.93	1740.8	5561.0	8.02E-02	—	91.5	8.24	30351.6
G5P29	A	0.54	11.96	7317.0	7766.6	2.79E-02	0.83	162.4	3.40	41790.9
G5P30	A	0.61	8.78	7610.3	5784.5	1.83E-02	0.75	120.5	2.39	13378.4
G5P32	S	1.50	0.77	19138.8	496.7	6.54E-04	0.27	140.0	1.33	42049.9
G5P33	S	1.40	1.47	18020.1	962.5	1.36E-03	0.45	150.7	1.51	42096.7
G5P34	S	1.60	1.97	20818.8	1352.0	1.67E-03	0.47	160.6	1.44	35737.7
G5P35	S	1.50	3.98	19418.4	2937.6	3.88E-03	0.65	195.7	1.85	54228.6
G5P36	S–A	0.75	6.93	9926.9	4556.2	1.20E-02	0.71	166.4	2.70	62086.9
G5P40	S–A	1.52	8.16	19115.0	7161.0	9.22E-03	0.79	204.8	1.95	33072.2

correlations may be expressed in terms of the single-phase Nusselt number (Nu_L) as:

$$\text{Laminar:}\quad Nu_L = \frac{h_L D}{k_L} = 1.86(Re_{SL}Pr_L D/L)^{0.33}\left(\frac{\eta_{L,b}}{\eta_{L,w}}\right)^{0.14} \qquad [4]$$

$$\text{Turbulent:}\quad Nu_L = \frac{h_L D}{k_L} = 0.023 Re_{SL}^{0.8} Pr_L^{0.33}\left(\frac{\eta_{L,b}}{\eta_{L,w}}\right)^{0.14} \qquad [5]$$

where k_L is the liquid thermal conductivity (W/m K), Pr_L is the liquid Prandtl number, and $\eta_{L,b}$ and $\eta_{L,w}$ are the dynamic viscosities (N s/m²) of the liquid at bulk fluid and tube wall conditions, respectively. A comparison of the single-phase heat transfer data from the flight apparatus with the correlations is shown in figure 3. In the figure, the experimental $1 - G$ and Sieder–Tate generated Nusselt numbers are plotted as functions of Re_{SL}. It can be seen that the agreement was good with RMS deviations of 14.9% for laminar flow and 9.9% for turbulent flow.

2.4. Measurement error and uncertainty

All the flight and ground heat transfer data that were collected over the course of this research project were utilized in an assessment of the total uncertainty of the normalized heat transfer coefficient ($\psi^2 = h_{TP}/h_L$). In this analysis, the bias uncertainties of the thermocouples used were 0.5°C and those of the RTD measurements were 0.26°C. The heater power measurement had an

uncertainty of approximately 1.1%. The liquid and gas flow measurements had biases of 1.0 and 1.8%, respectively.

It was found that the total uncertainty in the measurements, including both the bias of the instrumentation and repeatability of ψ^2 for the entire data set of flight and ground experiments was 14.3% for $Re_{SL} > 2300$ and 6.4% for $Re_{SL} < 2300$. Details on this uncertainty analysis may be found in Rite and Rezkallah (1994a) and Rite (1995).

3. EXPERIMENTAL RESULTS

3.1. *Nusselt numbers: 1 − G vs μ − G*

An examination of the effect of gravity was first made by comparing the two-phase heat transfer coefficients gathered in-flight ($\mu - G$) with those obtained on-ground ($1 - G$) using the same apparatus. The results of this comparison for air–water data are shown in figures 4–7. In the figures, the two-phase Nusselt number (Nu_{TP}), defined as:

$$Nu_{TP} = \frac{h_{TP} D}{k_L} \qquad [6]$$

(where k_L is the thermal conductivity of the liquid) is plotted as a function of gas quality (x). The latter was determined from the independent measurements of liquid and gas mass flowrates.

Data at superficial liquid velocities "V_{SL}" of approximately 0.07, 0.10, 0.24, 0.41, 0.89, 1.5 and 2.5 m/s with V_{SG} varying from 0.1 to 26 m/s are presented. The flow regime associated with the set point is also marked beside each data point. The abbreviations for the various flow regimes are as follows: B: bubbly, S: slug, C: churn, S–A: froth slug–annular (transitional), and A: annular. Tabular listings of the results from the 1994 flight and ground data are presented in tables 2 and 3, respectively. In the tables, flow regime, V_{SL}, V_{SG}, Re_{SL}, Re_{SG}, x, gas void fraction (ϵ), Nu_{TP} and ψ^2 are given for the flight and ground data. The gravity ratio (g/g_0) is also provided for the flight data.

It can be seen in figures 4–7 that at low liquid velocities and low gas qualities (mainly in the low gas quality slug flows), the $1 - G$ Nusselt number values are greater than those measured at $\mu - G$ for the same liquid flowrates. This was also found to be the case at higher liquid flowrates in the bubbly flow regime (figure 7). As the gas flowrate is increased (thus moving to annular flow

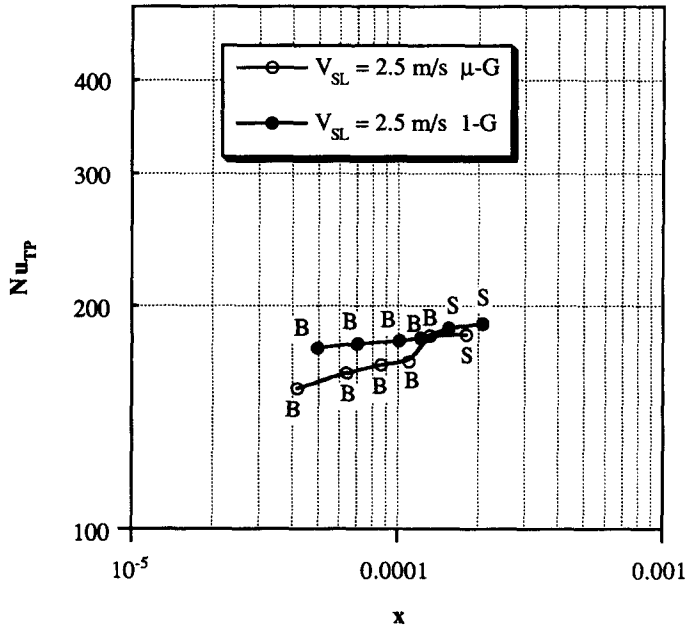

Figure 7. $1 - G$ and $\mu - G$ average Nu_{TP} vs gas-quality: $V_{SL} \approx 2.5$ m/s.

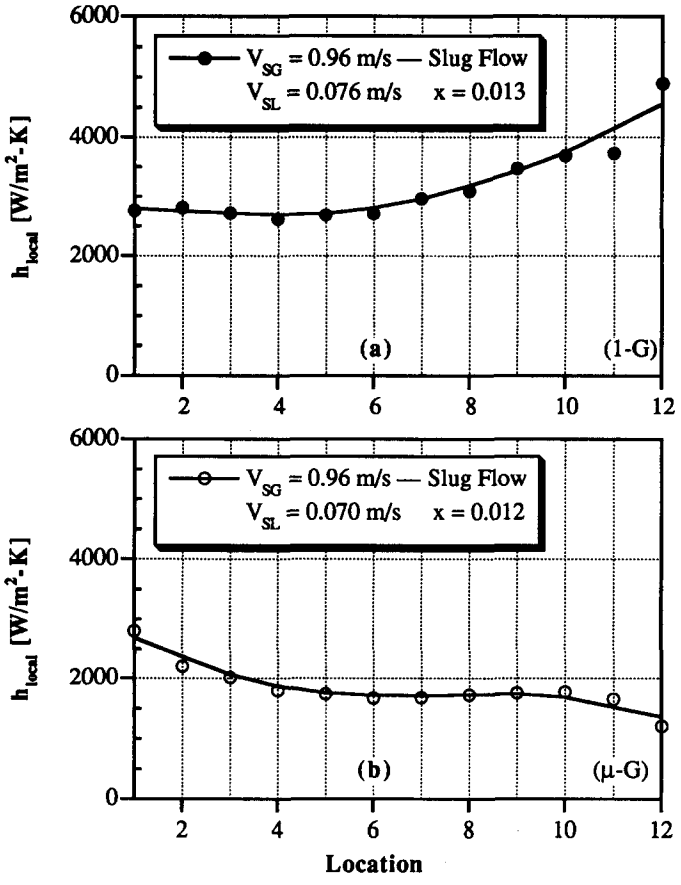

Figure 8. Local, two-phase heat transfer coefficients: $V_{SL} \approx 0.07$ m/s, (a) $1 - G$, (b) $\mu - G$.

conditions with high gas inertia), the $1 - G$ and $\mu - G$ data points approach one another until they become very nearly the same. This suggests that the difference between $1 - G$ and $\mu - G$ behavior is flow regime dependent. Hence, further analysis will be presented with reference to the flow regime associated with the flow. It should also be noted that, recalling the magnitude of the uncertainty in the measurement, the differences in the heat transfer coefficients at $1 - G$ and $\mu - G$ are much larger than the uncertainty only at very low liquid velocities and low qualities, mostly in the low gas quality slug flows.

4. ANALYSIS OF RESULTS

4.1. Local heat transfer coefficients

The first step taken in the analysis of the heat transfer results was an examination of local heat transfer coefficients. The results of this investigation are shown graphically in figures 8–11 for air–water at both $1 - G$ and $\mu - G$ conditions. In these figures, the local heat transfer coefficients (h_{local}) calculated from each of the twelve surface temperature measurements on the heated test section are plotted as functions of location from inlet to outlet (stations 1–12). Only bubbly and slug flow regime data from the 1994 flight campaign are shown.

Figure 8(a) and (b) show the local convective coefficients for $V_{SL} \approx 0.07$ m/s ($Re_{SL} \approx 840$) and a superficial gas velocity of 0.96 m/s in the slug flow regime for $1 - G$ and $\mu - G$ conditions ($x \approx 0.013$ and 0.012, respectively, as presented in figure 4). It can be seen that for $1 - G$ flows the local heat transfer coefficient increases from entrance to exit. At $\mu - G$ conditions in figure 8(b), the inlet heat transfer coefficients are higher than the values near the exit. This indicates that under $\mu - G$ conditions there is a relatively long thermal entry length as one would expect for laminar conditions in single-phase flows, Kays and Crawford (1980). But, for low gas flows under $1 - G$ something is disturbing the fluid layer at the wall and minimizing the thermal entry length.

Figure 9(a) and (b) show the results at a constant V_{SL} of 0.10 m/s ($Re_{SL} \approx 1200$). In these figures, slug flow is present in both cases at $V_{SG} = 0.14$ m/s ($x \approx 0.0015$ and 0.0013, respectively, as presented in figure 4). The $1 - G$ data shows, once again, an increase in the local heat transfer coefficient from inlet to outlet while the $\mu - G$ results show the opposite. Thus indicating that the thermal entry length for $\mu - G$ is significantly longer, analogous to single-phase forced-convective flows.

A further increase in the superficial liquid velocity to 0.24 m/s ($Re_{SL} \approx 2900$) yields similar results; these are shown in figure 10(a) and (b). The profiles for $1 - G$ and $\mu - G$ at a gas flowrate of $V_{SG} = 0.09$ m/s in the slug flow regime are presented in the figures ($x \approx 0.00044$, 0.00035, respectively, as presented in figure 5). The heat transfer coefficient profiles in this case, however, are beginning to more closely resemble one another as the liquid flowrate increases.

Finally, at $V_{SL} \approx 0.4$ m/s ($Re_{SL} \approx 4900$) as shown in figure 11(a) and (b), both trends and values of the $1 - G$ and $\mu - G$ data are similar for $V_{SG} = 0.19$ m/s ($x \approx 0.00060$, and 0.00047, respectively, as presented in figure 5). The scatter of heat transfer coefficients along the length of the tube, which has been observed earlier at the highest gas flows, is an artifact of the heater wire due to a small non-uniformity in the wire-wrapping and the thermocouple placement. Despite this, it is apparent that a more uniform profile is developing as would be characteristic of fully turbulent, single-phase flows. It should be remembered that superficial velocities are being used to determine the liquid Reynolds numbers, and the actual liquid Reynolds numbers may be higher due to the reduced liquid flow area as will be discussed later.

It appears that under $1 - G$ conditions the gas is influencing the local heat transfer by disturbing the liquid flow at the wall of the tube. This agrees with the findings of Vijay *et al.* (1978), who hypothesized that the effect of buoyancy forces on the gas bubbles caused the gas to have a greater velocity than the surrounding liquid. This "slip" between the phases led to a break-down in the laminar sub-layer near the tube wall, thus leading to a movement away from laminar flow-type

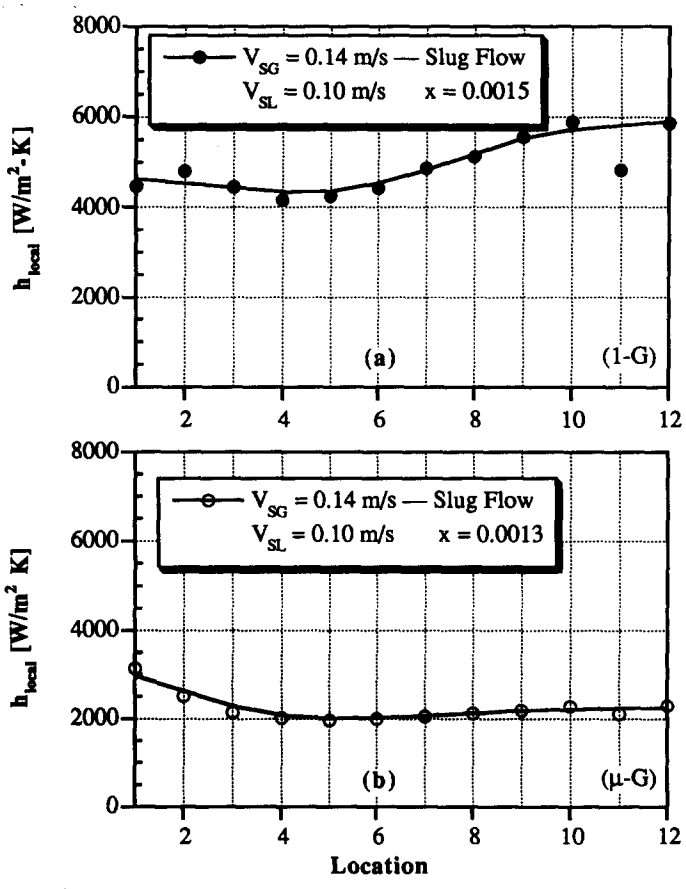

Figure 9. Local, two-phase heat transfer coefficients: $V_{SL} \approx 0.10$ m/s, (a) $1 - G$, (b) $\mu - G$.

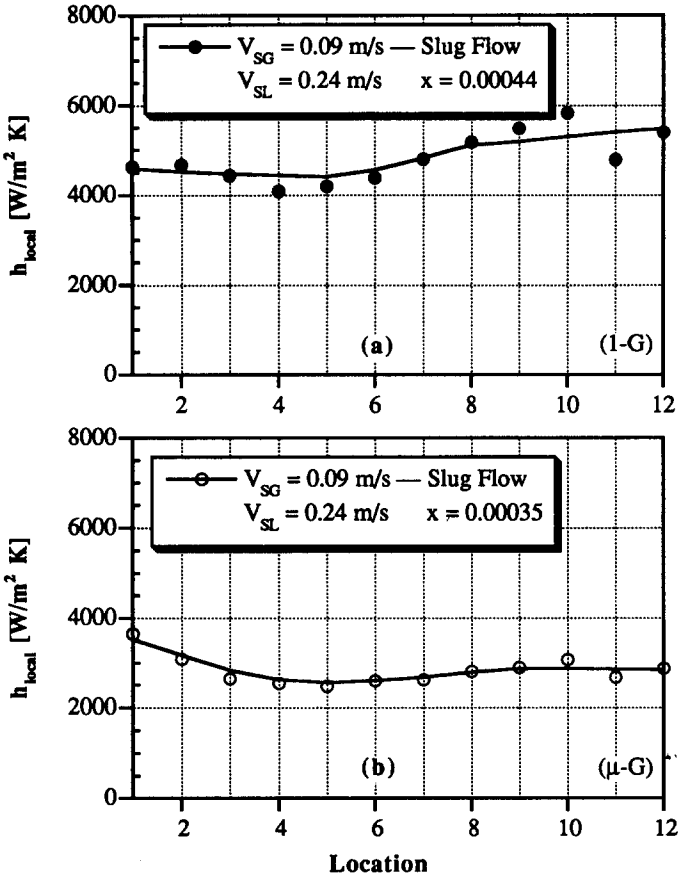

Figure 10. Local, two-phase heat transfer coefficients: $V_{SL} \approx 0.24$ m/s, (a) $1 - G$, (b) $\mu - G$.

behavior. However, under $\mu - G$ conditions this would not happen. The reduction of gravity greatly lessens the buoyancy forces and therefore the turbulence-generating ability of the gas bubbles. The bubbles at $\mu - G$ flow mainly at the center of the tube, and therefore they do not seem to interfere with the laminar sub-layer.

The work of Serizawa *et al.* (1975), as well as many others, further supports the hypothesis of Vijay *et al.* (1978). Serizawa *et al.* (1975) reported for air–water flows through a 17.5 mm diameter vertical tube a "saddle-shaped" void fraction distribution. For bubbly flow, the bubbles were distributed such that the largest concentration was very near the tube wall. As the flow changed to slug flow, the void fraction distribution moved toward a more "bullet-shaped" profile with a maximum at the tube centerline. This concentration of bubbles near the tube wall would account for the disturbance of the sub-layer at the wall.

More recently, a difference in the void distribution at $1 - G$ and $\mu - G$ has been reported by Kamp *et al.* (1993). In this work, void distributions for air–water up-flow through a vertical tube with a diameter of 40 mm were reported. Superficial liquid velocities ranging from 0.27 to 0.99 m/s with superficial gas velocities of 0.023 and 0.044 m/s were tested. Comparing results obtained in the laboratory at $1 - G$ conditions with those for $\mu - G$ conditions aboard a low-gravity aircraft, they also found that the "saddle-shaped" distribution of Serizawa was present at $1 - G$, but not at $\mu - G$.

4.2. Proposed heat transfer model

It was noted above that the $\mu - G$ heat transfer results for the bubbly and slug flow regimes are very similar to the single-phase thermal entry length profiles. It is therefore logical to consider the possibility of modelling the two-phase results with previous single-phase solutions using the appropriate Reynolds number definition. In order to consider this theory, the $\mu - G$ results shown

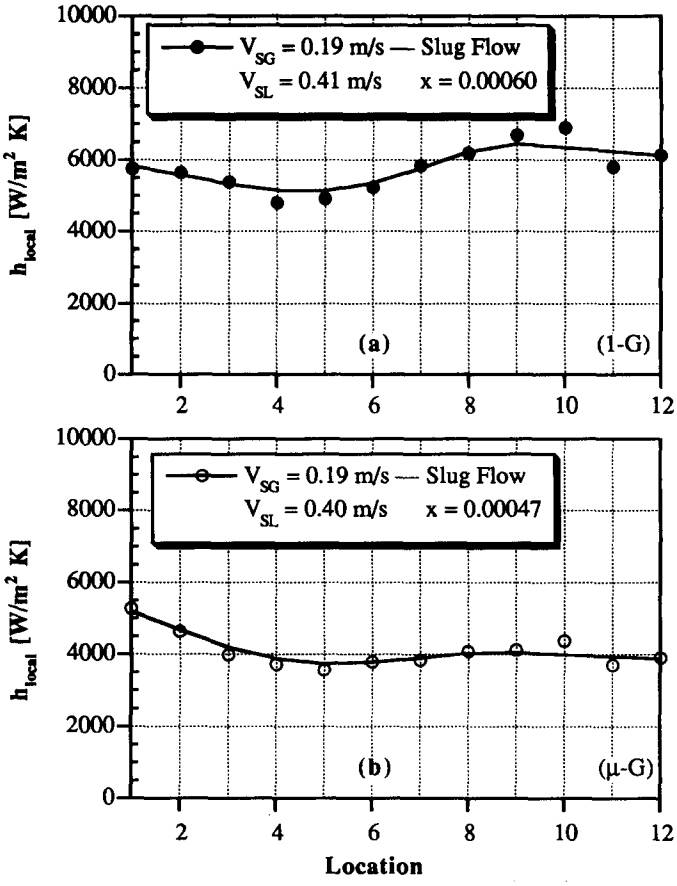

Figure 11. Local, two-phase heat transfer coefficients: $V_{SL} \approx 0.41$ m/s, (a) $1 - G$, (b) $\mu - G$.

above were compared with well-known single-phase solutions for thermal entry length internal flows. Since it has been shown in the previous section that the interaction of the gas-phase with the near-wall liquid layer is minimal at $\mu - G$, it is not clear whether a two-phase Reynolds number or a superficial liquid Reynolds number should be used in these comparisons to best represent the internal flow. If the gas bubbles remain at the center of tube, the acceleration of the liquid layer at the wall as well as the turbulence generation there should be minimal. Therefore, the comparisons

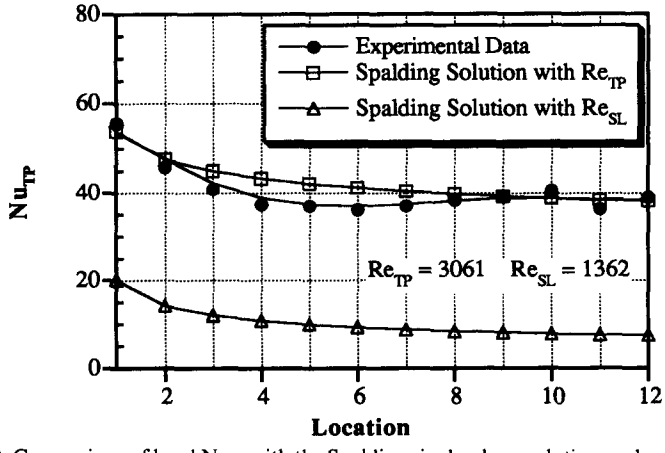

Figure 12. Comparison of local Nu_{TP} with the Spalding single-phase solution evaluated with Re_{TP} and Re_{SL}: $Re_{TP} = 3061$ and $Re_{SL} = 1362$.

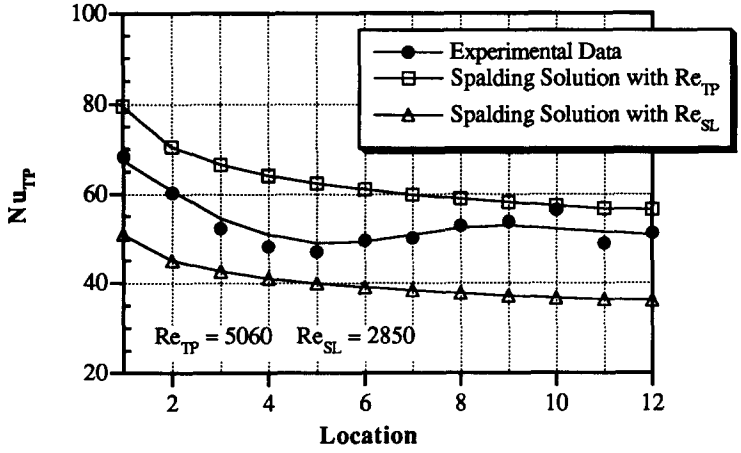

Figure 13. Comparison of local Nu_{TP} with the Spalding single-phase solution evaluated with Re_{TP} and Re_{SL}: $Re_{TP} = 5060$ and $Re_{SL} = 2850$.

were made using both the superficial Reynolds number given in [1] and a two-phase Reynolds number (Re_{TP}) defined as:

$$Re_{TP} = \frac{Re_{SL}}{(1-\epsilon)} \quad [7]$$

where ϵ is the gas void fraction measured *in situ* with a capacitance-type sensor, details of which can be found in Elkow (1995), and listed in tables 2 and 3. For the comparisons using Re_{TP}, mixture properties based on a quality-weighted average were used to evaluate the Nusselt numbers from the various models. These properties were calculated using the equation:

$$\zeta_{MIX} = x\zeta_G + (1-x)\zeta_L \quad [8]$$

where ζ_{MIX} (density, viscosity, thermal conductivity, and specific heat) is the physical property of the mixture, x is the gas mass-quality, ζ_G is the physical property of the gas (air), and ζ_L is the physical property of the liquid (water).

Based on the above definition of Reynolds number, it was found that for $Re_{TP} < 2300$ the application of laminar, analytical, single-phase thermal entry length solutions (Kays and Crawford 1980) to two-phase $\mu - G$ data resulted in underprediction of the local heat transfer coefficients by up to 60–70% for the data points in this Reynolds number range. However, application of the turbulent analytical thermal entry length solution of Spalding (1961) to data between $3000 < Re_{TP} < 10{,}000$ was found to give much better results. A lower limit of 10,000 was chosen

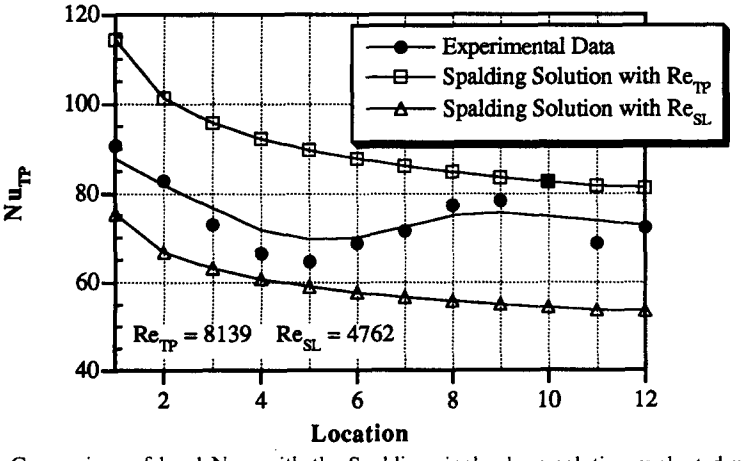

Figure 14. Comparison of local Nu_{TP} with the Spalding single-phase solution evaluated with Re_{TP} and $Re_{SL} = 8139$ and $Re_{SL} = 4762$.

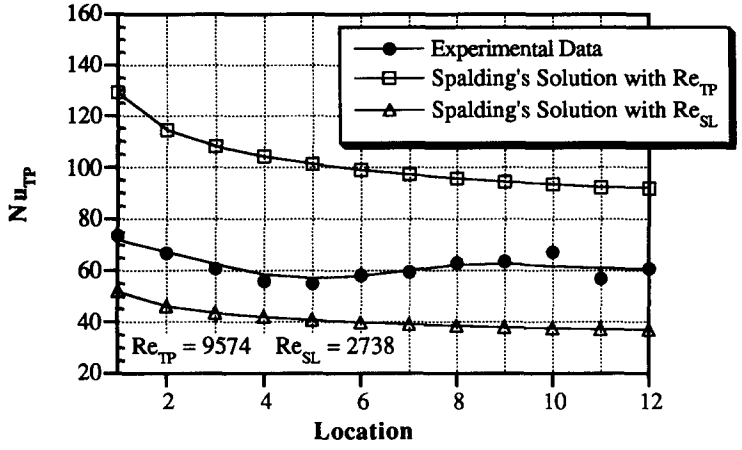

Figure 15. Comparison of local Nu_{TP} with the Spalding single-phase solution evaluated with Re_{TP} and Re_{SL}. $Re_{TP} = 9574$ and $Re_{SL} = 2738$.

based on the average Nusselt number values given in figures 4–7. In the figures, the $1 - G$ Nusselt numbers are significantly higher than the $\mu - G$ values up to a Re_{TP} of approximately 10,000.

The solution of Spalding (1961) applies to heat transfer to a turbulent stream with a step-wise discontinuity in wall temperature. In this work, the heat transfer coefficient is expressed in terms of Stanton number. The Stanton number may be expressed as:

$$\mathrm{St} = \frac{h}{\rho C_p V} \qquad [9]$$

where C_p is the specific heat (J/kg K) and V is the fluid velocity (m/s), which was evaluated as V_{SL} and V_{TP} based on Re_{TP} for the purposes of this paper.

A non-dimensional axial coordinate, x^+, is then defined based on the integral:

$$x^+ = \int_1^x V \frac{\sqrt{C_f/2}}{\nu} \, dx \qquad [10]$$

where ν is the kinematic viscosity (m^2/s). The coefficient of friction, C_f, was approximated by the Blasius solution given by Schlichting (1979) as:

$$C_f = \frac{0.3164}{\mathrm{Re}^{0.25}}. \qquad [11]$$

Once again, Re was evaluated as Re_{SL} and Re_{TP}.

A value of x^+ for each of the 12 differential elements of the heated test section was calculated. The approximate analytical solution of Lighthill (1950) for $x^+ < 300$ was used to solve for Stanton number. Lighthill's solution is as follows:

$$\frac{\mathrm{St}}{\sqrt{C_f/2}} = 0.538(x^+)^{-1/3}. \qquad [12]$$

For $x^+ > 300$, the approximation of Reynolds *et al.* (1958) and Seban (1951) was used. Their solution may be expressed as:

$$\frac{\mathrm{St}}{\sqrt{C_f/2}} = 0.1432(x^+)^{-1/9}. \qquad [13]$$

Since both the Lighthill and Seban–Reynolds solutions are for fluids with $Pr = 1$, in order to account for the higher Prandtl number in the present study the results calculated above were multiplied by $Pr^{-2/3}$ as recommended by Spalding.

The results of the comparison of Spalding's solution evaluated with Re_{TP} and Re_{SL} are shown in figure 12 for the $\mu - G$ slug flow regime case of $V_{SL} = 0.11$ m/s and $V_{SG} = 0.19$ m/s ($Re_{TP} = 3061$,

$Re_{SL} = 1362$, and $x = 0.0015$), figure 13 for the $\mu - G$ slug flow regime case of $V_{SL} = 0.24$ m/s and $V_{SG} = 0.19$ m/s ($Re_{TP} = 5060$, $Re_{SL} = 2850$, and $x = 0.00074$), figure 14 for $V_{SL} = 0.40$ m/s with $V_{SG} = 0.34$ m/s ($Re_{TP} = 8139$, $Re_{SL} = 4762$, and $x = 0.00080$) and, figure 15 for $V_{SL} = 0.24$ m/s with $V_{SG} = 0.64$ m/s ($Re_{TP} = 9574$, $Re_{SL} = 2738$, and $x = 0.0024$). In the figures, the experimentally measured local Nusselt numbers and the predictions made from the Spalding model with Re_{SL} and Re_{TP} are plotted as functions of location in the heated test section. It can be seen that the Spalding model heat transfer coefficient profiles compare favorably with the experimental data, with the latter falling between the solutions using Re_{TP} and with Re_{SL} as the basis of calculations. For all flight data with Re_{TP} between 3060 and 9580, the arithmetic mean deviation between the Spalding model with Re_{TP} and the experimental results for all of the flow cases is approximately +27%. The RMS deviation between the prediction and the actual results is 46%. Evaluating Spalding's model using Re_{SL} over the same range, the average and RMS deviations are −11% and 26%, respectively. This indicates that the actual Reynolds number of the mixture is in fact a value between those calculated based on the superficial and the two-phase velocities. Local velocity measurements are needed to quantify the basis of the appropriate average.

For data with $Re_{TP} > 10{,}000$, the predictions of the Spalding model (using both Re_{SL} and Re_{TP}) were quite poor. This may be explained by the fact that above $Re_{TP} = 10{,}000$ the local Nusselt numbers are essentially uniform with the difference between the inlet and outlet coefficients being less than 20% (i.e. Nu_{local} approaches Nu_{∞}). This is the criterion that was used by Vijay *et al.* (1978) for the applicability of their Graetz number solutions. It was found, however, that the Sieder–Tate empirical turbulent flow correlation (given in [5]) compares well with the data at these higher flowrates, having an RMS deviation of 23% and a mean deviation of +13%. It is clear that for bubbly and slug flows under $\mu - G$ where slip between the gas and liquid is minimal, treatment of the flow as a single-phase fluid with appropriately defined mixture properties is a viable method of predicting heat transfer.

5. SUMMARY AND CONCLUSIONS

Based on a large pool of two-phase heat transfer data points that have been collected both in-flight and on-ground, several new and interesting conclusions have been reached. These results may be summarized as follows:

(1) For two-phase Reynolds numbers (Re_{TP}) less than 10,000, $\mu - G$ reduces the heat transfer coefficient by up to 50% in the slug flow regime compared with $1 - G$. As the gas-quality is increased, the difference between $1 - G$ and $\mu - G$ data becomes smaller.

(2) At higher liquid flowrates ($Re_{TP} > 10{,}000$), for very low qualities there is again a tendency for the $1 - G$ heat transfer coefficients to be greater than those at $\mu - G$. The two approach one another until above $x \approx 0.002$, the $\mu - G$ heat transfer data are greater than the $1 - G$. However, the magnitude of the difference is on the order of 10–15%, which is slightly higher than the uncertainty of the measurements.

(3) Analytical single-phase thermal entry length solutions were investigated to predict two-phase heat transfer behavior under microgravity conditions. Using the turbulent solutions of Spalding, it was found that agreement with the experimental data is within ±46% with two-phase Reynolds numbers between 3000 and 10,000. Evaluating the model using Re_{SL}, based on the liquid superficial velocity, the experimental Nusselt numbers were underpredicted by only 11%. An evaluation with the two-phase mixture Re_{TP} resulted in overprediction by 27%. Therefore, an average Reynolds number based on local velocity measurements in the near wall liquid layer is needed to more accurately predict two-phase microgravity heat transfer. For flows with $Re_{TP} > 10{,}000$, where a uniform heat transfer profile from inlet to outlet is apparent, the empirical model of Sieder–Tate for single-phase flow was found to predict heat transfer within ±23%.

Acknowledgements—The authors gratefully acknowledge the financial assistance of the Microgravity Sciences Division of the Canadian Space Agency (CSA), the Natural Sciences and Engineering Research Council of Canada (NSERC), and the University of Saskatchewan.

REFERENCES

Elkow, K. (1995) Void fraction measurement and analysis at normal gravity and microgravity conditions, M.Sc. Thesis, University of Saskatchewan, Saskatoon.

Feldmanis, C. J. (1966) Pressure and temperature changes in closed loop forced convection boiling and condensing processes under zero gravity conditions. *Institute of Environmental Sciences' 1966 Annual Technical Meeting Proceedings*.

Kakaç, S. (1987) The effect of temperature-dependent fluid properties on convective heat transfer. *Handbook of Single-phase Convective Heat Transfer*, ed. S. Kakaç, R. K. Shah and W. Aung. Wiley, New York.

Kamp, A., Colin, C. and Fabre, J. (1993) Bubbly flow in a pipe: Influence of gravity upon void and velocity distribution. *3rd World Conference on Experimental Heat Transfer, Fluid Mechanics, and Thermodynamics*, Honolulu, HI, 30 October–5 November.

Kays, W. M. and Crawford, M. E. (1980) *Convective Heat and Mass Transfer*, 2nd Edition, pp. 103–113, 260–270. McGraw-Hill, New York.

Kays, W. M. and Perkins, H. C. (1985) Forced convection, internal flow in ducts. *Handbook of Heat Transfer Fundamentals*, 2nd Edition, ed. W. M. Rohsenow, J. P. Hartnett and E. N. Ganic. McGraw-Hill, New York.

Lighthill, M. J. (1950) Contributions to the theory of heat transfer through a laminar boundary layer. *Proc. Roy. Soc. A* **202,** 359.

Ohta, H., Fujiyama, H., Inoue, K., Yamada, Y., Ishikura, S. and Yoshida, S. (1994) Microgravity flow boiling in a transparent tube. *10th International Heat Transfer Conference*, Brighton, England, No. 111.

Papell, S. S. (1962) An instability effect on two-phase heat transfer for subcooled water flowing under conditions of zero gravity. *American Rocket Society 17th Annual Meeting and Space Flight Exposition*.

Reinarts, T. R., Best, F. R. and Hill, W. S. (1992) Definition of condensation two-phase flow behaviors for spacecraft design. *AIP Conference Proc. No. 246*, Vol. 1, pp. 1216–1225. American Institute of Physics, New York.

Reynolds, W. C., Kays, W. M. and Kline, S. J. (1958) Heat transfer in the turbulent incompressible boundary layer, II—The step wall-temperature distribution. NASA Memo 12-2-58 W.

Rite, R. W. (1995) Heat transfer in gas–liquid flows through a vertical, circular tube under microgravity conditions, Ph.D. Thesis, University of Saskatchewan, Saskatoon.

Rite, R. W. and Rezkallah, K. S. (1994a) Heat transfer in two-phase flow through a circular tube at reduced gravity. *J. Thermophysics and Heat Transfer* **8,** 702–708.

Rite, R. W. and Rezkallah, K. S. (1994b) The influence of liquid viscosity on heat transfer coefficients in gas–liquid flows under microgravity conditions. *AIP Conference Proc. No. 301*, Vol. 1, pp. 1129–1136. American Institute of Physics, New York.

Rite, R. W. and Rezkallah, K. S. (1993) An investigation of transient effects on heat transfer measurements in two-phase gas–liquid flows under microgravity conditions. *ASME Heat Transfer in Microgravity Systems*, pp. 49–57.

Schlichting, H. (1979) *Boundary-layer Theory*, 7th Edition, p. 597. McGraw-Hill, New York.

Seban, R. (1951) Experimental investigation of convective heat transfer to air from a flat plate with a step-wise discontinuous surface temperature, M.S. Thesis, University of California, Berkeley.

Serizawa, A., Kataoka, I. and Michiyoshi, I. (1975) Turbulence structure of air–water bubbly flow—II. Local properties. *Int. J. Multiphase Flow* **2,** 235–246.

Spalding, D. B. (1961) Heat transfer to a turbulent stream from a surface with a step-wise discontinuity in wall temperature. *Int. Dev. Heat Transfer Part I*, International Heat Transfer Conference, Boulder, CO, pp. 439–446.

Vijay, M. M., Savic, P. and Sims, G. E. (1978) The Graetz problem for two-phase two-component gas–liquid flow in vertical tubes. *6th International Heat Transfer Conference*, Toronto, Canada, 7–11 August 1978, Vol. 1, pp. 493–497. Hemisphere, Washington, DC.